Dynamics of PAHs and derived organic compounds in a soil-plant mesocosm spiked with 13C-phenanthrene

Johanne Cennerazzo, Alexis de Junet, Jean-Nicolas Audinot, Corinne Leyval

Dynamics of PAHs and derived organic compounds in a soil-plant mesocosm spiked with ^{13}C-phenanthrene.

Johanne Cennerazzo[a,b], Alexis de Junet[a,b], Jean-Nicolas Audinot[c], Corinne Leyval[a,b]

[a]*Université de Lorraine, Laboratoire Interdisciplinaire des Environnements Continentaux, UMR 7360, Vandœuvre-lès-Nancy, F-54506, France*

[b]*CNRS, Laboratoire Interdisciplinaire des Environnements Continentaux, UMR 7360, Vandœuvre-lès-Nancy, F-54506, France*

[c] *Advanced Instrumentation for Ion Nano-Analytics, Materials Research and Technology Department, Luxembourg Institute of Science and Technology, 41 rue du Brill , L-4422, Luxembourg*

Abstract

Polycyclic Aromatic Hydrocarbons (PAHs) are ubiquitous and persistent soil pollutants. Their fate and the influence of the plant rhizosphere on their dynamics has been extensively studied, but studies mainly focused on their dissipation rate. We conducted a plant-soil mesocosm experiment to study the fate and distribution of PAHs or derived compounds in the extractable fraction, the residual soil, the shoot biomass and the root biomass. The experiment was conducted for 21 days using ryegrass and a forest soil spiked with ^{13}C-labeled phenanthrene (PHE), using combined IRMS and NanoSIMS for analyses. Almost 90% of the initial extractable PHE content was dissipated within 3 weeks, but no rhizospheric effect was highlighted on PHE dissipation. More than 40% of ^{13}C-PHE was still in the soil at the end of the experiment, but not as PHE or PAH-derived compounds. Therefore it was under the form of new compounds (metabolites) and/or had been incorporated into the microbial biomass.

About 0.36% of the initial ^{13}C-PHE was recovered in the root and shoot tissues, representing similar ^{13}C enrichment ($E^{13}C$) as in the soil ($E^{13}C \approx 0.04$ at.%). Using NanoSIMS, ^{13}C was also localized at the microscale in the roots and their close environment. Global ^{13}C enrichment confirmed the results obtained by IRMS. Some hotspots of ^{13}C enrichment were found, with a high $^{32}S/^{12}C^{14}N$ ratio. Comparing the ratios, sizes and shapes of these hotspots suggested that they could be bacteria.

Keywords: Polycyclic Aromatic Hydrocarbons; ^{13}C-Phenanthrene; soil; rhizosphere; IRMS; NanoSIMS

Highlights:

- A mesocosm experiment with ^{13}C-PHE-spiked soil was analyzed by IRMS and NanoSIMS
- 40% of ^{13}C-PHE was still in the soil after 21 days but not as the parent compound
- Bacterium-like ^{13}C-enriched hotspots were revealed by NanoSIMS close to the roots

1. Introduction

Polycyclic Aromatic Hydrocarbons (PAHs) are ubiquitous and persistent organic compounds found in the soils of large brownfield areas in many former industrial regions. They are composed of two or more benzene rings and result from the incomplete combustion by pyrolysis of organic materials from natural or anthropogenic sources (Edwards, 1983). They are persistent in soils due to their low water solubility and high adsorption on soil constituents (Wilson and Jones, 1993). They are harmful to human and environmental health, and 16 of them are listed as priority pollutants by the USEPA (Hartmann, 1996).

Many studies have addressed the fate and dynamics of PAHs in soils, where they can undergo numerous processes such as plant uptake, stabilization by sorption on organic and mineral phases, or transformation and degradation until total mineralization. Sorption and degradation are key processes in the fate of PAHs in the environment (Magee et al., 1991). The persistence of organic pollutants in soils has been attributed to sequestration mechanisms including intra-organic matter and intra-particle diffusion of the parent compound and transformation products (Doick et al., 2005). Plants seem to have a limited direct impact on PAH dynamics in polluted soils (Fang et al., 2001; Günther et al., 1996; Rezek et al., 2008). Gao and Zhu (2004) showed that uptake of phenanthrene and pyrene by plants accounted for less than 0.01 and 0.23% of enhanced loss in vegetated versus non-vegetated soils. The low water solubility of PAHs could prevent significant uptake by plant tissues (Binet et al., 2000; Kipopoulou et al., 1999) and root-to-shoot translocation (Burken and Schnoor, 1998). However, the indirect role of plants in PAH dynamics through their root systems is largely documented (Rezek et al., 2008; Miya and Firestone, 2000; Liste and Alexander, 2000). The plant rhizosphere is a favorable environment for high microbial diversity and activity, which permit higher PAH dissipation in soils (Corgié et al., 2003; Anderson et al., 1993; Schwab, 1994; Reilley et al. 1996). The main mechanisms involved in PAH dissipation in the soil and the rhizosphere are biodegradation and biotransformation by an active microflora (Binet et al., 2000; Wilson and Jones 1993; Cerniglia, 1997). The soil heterotrophic microflora may use organic pollutants as a source of carbon (C) and energy to grow, or for co-metabolism (Hwang and Cutright, 2002). The C derived from PAHs (C-PAH) could be (i) incorporated into the microbial biomass (Kästner et al., 1999), and/or (ii) transformed into other organic compounds and thus form part of non-extractable PAHs (Richnow et al., 1998 and 1999). The newly formed organic products could be more reactive than the parent compounds and therefore bind with soil components more easily, but could also be more toxic (Sabaté et al., 2006). Cébron et al.

75 (2011) showed that 38% of the ^{13}C from labeled PAH added into soil mesocosms was not
76 extractable after 12 days. C-PAH was still present but probably not under the form of parent
77 PAHs or extractable compounds. Some of these newly formed organic compounds may be more
78 soluble and more mobile than parent PAHs (Sabaté et al., 2006). However, most of the studies
79 led so far only considered the dissipation of PAHs in the soil and in the plant rhizosphere. Some
80 studies focused on the residual and newly formed organic compounds, especially on the
81 distribution and the dynamics of C-PAH in the soil (Doick et al., 2005; Eschenbach et al., 1998;
82 Kästner et al., 1999; Macleod and Semple, 2003; Northcott and Jones, 2001; Richnow et al.,
83 1998), but no in soil-plant-microflora compartments.

84 An effective and relevant way to trace carbon compounds in soil-plant ecosystems is to
85 use ^{13}C isotopic labeling. For example, Richnow et al. (2000, 1998) used [1-^{13}C]-PAH to trace
86 the transformation of phenanthrene in a soil reactor. But it appears more relevant to monitor C-
87 PAH using a molecule labeled on all its carbon atoms (Cébron et al., 2011). Another
88 complementary method to trace a labeled organic compound in soils, plants or bacteria is to
89 map isotopic distribution at a microscale through NanoSIMS analyses (high-resolution imaging
90 Secondary Ion Mass Spectrometry) (Hoppe et al., 2013). NanoSIMS analyses can map all the
91 elements (isotopes) of the periodic table with an ultimate lateral resolution (probe size) in the
92 50 to 150 nm range, high sensivity (a few ppm), and high mass resolution (Herrmann et al.,
93 2007; Moore et al., 2012; Remusat et al., 2012; Vidal et al., 2016).

94 The objective of our study was to investigate the fate of C-PAH in planted and non-planted
95 soil by assessing (i) the distribution of C-PAH in the extractable fraction, the residual soil, the
96 shoot biomass and the root biomass, and (ii) the localization of C-PAH in different
97 compartments of the soil-plant system. We conducted a mesocosm trial using ryegrass, ^{13}C-
98 phenanthrene (^{13}C-labeled on all its carbon atoms) soil spiking, and coupling isotopic analyses
99 with NanoSIMS analyses.

2. Materials & methods

2.1. Soil-plant mesocosms

Planted and non-planted mesocosms were set up, with soil spiked with either unlabeled ^{12}C-PHE (control) or labeled ^{13}C-PHE. The soil was a Calcisol, sampled at 5-35 cm depth in a temperate beech forest close to a former coking plant (49°14.163'N, 6°0.116'E, Homecourt, Lorraine region, France). The soil horizon had a pH_{water} of 7.3; it contained 48% clay, 44% silt, 7% sand, had organic carbon and total nitrogen contents of 23.0 and 1.62 g kg^{-1} respectively, and a low PAH content (13.4 mg kg^{-1}). The soil sample was air-dried, ground and sieved to 2 mm, and then spiked with 300 mg PHE kg^{-1} of soil. Spiking modalities were as follows: one with unlabeled PHE (^{12}C-PHE, Sigma Aldrich >97%) and two with known ^{13}C-PHE/^{12}C-PHE mixtures (^{13}C-PHE, Sigma-Aldrich Isotec Stables Isotopes, Miamisburg, Ohio, USA). The ^{13}C-PHE/^{12}C-PHE ratio was 1:8 for organic carbon analyses and 1:1 for NanoSIMS analyses. A PHE-hexane solution was added to 1:10 of the total soil mass for spiking. Hexane was evaporated under a fumehood, and then the spiked soil was homogenized with the remaining 9:10 of soil mass.

The planted and non-planted mesocosms were conducted in 50-mL glass jars with 40 g of PHE-spiked soil. They were inoculated with 10 mL of soil suspension from a PAH-contaminated soil (200 g L^{-1} in 0.85% NaCl) to ensure that a PAH-degrading microflora was present. Five ryegrass (*Lolium perenne*) seeds were added in each planted mesocosm. The experiment was conducted in a growth chamber under controlled conditions (22°C/18°C with 16h/8h day/night, 250 μmol photons m^{-2} s^{-1}, 80% relative humidity) for 21 days. Four replicates were prepared for each planted and non-planted modality and each sampling time (0, 7, 14 and 21 days), and for each ^{12}C-PHE- and ^{13}C-PHE/^{12}C-PHE- (1:8 ratio) spiked soil, except for 1:1 ^{13}C-PHE/^{12}C-PHE-spiked soil (one replicate, and sampling after 7 and 14 days for NanoSIMS microprobe analyses). At each sampling time, ryegrass shoots and roots were removed from

125 the soil and separated. The roots were washed with distilled water and dried with filter paper.
126 The fresh plant material and soil were oven-dried at 35 °C and then ground, and the soil was
127 sieved to 200 μm prior to analyses. The roots were prepared directly after sampling for
128 elemental mapping analyses.
129

130 2.2. Organic and isotopic analyses

131 PHE was extracted from 2 g of dry soil using dichloromethane (DCM) and a high-
132 pressure and high-temperature DIONEX® 200 ASE (Accelerated Solvent Extractor) automated
133 extractor. Residual soil (after PAH extraction) was kept for organic analyses. DCM was
134 evaporated from the PAH extracts under N_2 flow and replaced by acetonitrile for PAH analysis.
135 PAH extracts were analyzed using a reverse-phase chromatography UHPLC Ultimate 3000
136 RSLC system (Dionex) equipped with a Diode Array Detector and a Zorbax Eclipse PAH
137 RRHD column (100 mm x 2.1 mm, 1.8 μm – Agilent). The mobile phase was a mixture of
138 water/acetonitrile in gradient mode, with a flow rate of 0.420 mL min^{-1}. The wavelength used
139 for detection was 254 nm.
140

141 Isotopic and elemental analyses were performed on bulk and residual soil (before and
142 after PAH extraction, respectively), and on ryegrass shoot and root biomass using EA-
143 GC/IRMS (Elementary analyzer – Isotope Ratio Mass Spectrometry 100, IsoPrime,
144 Manchester. EA: IsotopeCube, Elementar, Hanau). Approximately 1.0 mg of the powdered
145 material of each sample was weighed and placed in 6x4 mm tin capsules (Elemental
146 Microanalysis Limited, Devon, UK). Analyses were carried out at the Technical Platform of
147 Functional Ecology (OC 081) at the INRA Forest Ecology and Eco-Physiology Unit. Isotopic
148 measurements were reported in the delta notation (δ expressed in ‰) as:

149 $$\delta\ ^{13}C\ (‰) = ((\frac{R_{sample}}{R_{Ref}}) - 1) \times 1000 \qquad \text{Eq. 1}$$

150 Where $R_{sample} = {}^{13}C_{sample}/{}^{12}C_{sample}$ for labeled and control samples, and R_{Ref} refers to the Vienna
151 Pee Dee Belemnite (VPDB) standard, with $R_{Ref} = {}^{13}C_{PDB}/{}^{12}C_{PDB} = 0.0112375$.
152 Enrichment in ^{13}C ($E^{13}C$), expressed as excess % of atoms (at.%), was calculated relatively to
153 the unlabeled control in the soil and in the plant, as follows:

154 $$E^{13}C\ (at.\%) = ({}^{13}C_{labeled} - {}^{13}C_{control}) \qquad \text{Eq. 2}$$

155 Where ${}^{13}C_{labeled}\ (at.\%) = [R_{labeled}/(R_{labeled}+1)] \times 100$, ${}^{13}C_{control}\ (at.\%) = [R_{control}/(R_{control}+1)] \times 100$.
156 $E^{13}C$ was calculated for bulk soil, residual soil, and ryegrass shoot biomass and root biomass.
157 Soil and plant ^{13}C concentrations ($^{13}C_{conc}$) were also calculated (expressed as μg C g^{-1} of soil and
158 μg C g^{-1} of plant, respectively):

159 $$^{13}C_{conc}\ (\mu g\ C\ g^{-1}) = (\frac{^{13}C_{(at.\%)} \cdot\ ^{13}C_{control}}{100}) \times C_x \qquad \text{Eq. 3}$$

160 Where C_x refers to the C content, expressed in μg C g^{-1} of soil or plant. ^{13}C distribution (%) in
161 the mesocosms was deduced from the ^{13}C concentrations and by considering that the percentage
162 of ^{13}C initially added in the soil after PHE-spiking was 100% (T0). ^{13}C distribution (%) was
163 calculated for the PAH extracts, the residual soil and the plants. The remaining ^{13}C was
164 considered as ^{13}C loss.

165 2.3. Elemental mapping analyses in the roots

166 The fresh ryegrass roots harvested after 7 and 14 days were rapidly cut into 0.5-cm
167 pieces and placed on adhesive film. The fine roots were cryofixed using a LEICA EM CPC
168 Universal Cryoworkstation. They were frozen at atmospheric pressure (10^5 °C s^{-1}), and
169 slammed on copper mirrors (Printz et al., 2016). Then the cryofixed samples were lyophilized
170 (LEICA EM CFD) without using any solvent (1°C h^{-1} for 8 days down to –20 °C at 1.10^{-4} Pa)
171 (Printz et al., 2016). The root samples were finally embedded in Epoxy resin and coated with
172 gold prior to analyses by nano Secondary Ion Mass Spectrometry.

Elemental mapping was performed using a Cameca NanoSIMS 50 ion probe (Gennevilliers, France) in the raster-imaging mode. The probe detects the secondary ions generated from each pulverized sample surface by an energetic incident ion beam (Hoppe et al., 2013). Ion images were obtained using a beam of Cs^+ primary ions with an energy impact of 16 keV and a beam current of 0.8 pA on the sample. The images were recorded in 256x256 pixels; under these conditions, a lateral resolution of 80-100 nm was expected. Negative secondary ion signals for $^{12}C^-$, $^{13}C^-$, $^{12}C^{14}N^-$, $^{32}S^-$ ions and $^{12}C^{14}N^-$, $^{56}Fe^{16}O^-$ clusters (Behrens et al., 2008) were collected simultaneously using the multicollection system. Images were acquired with a counting time of 30 ms/pixel. Mass resolution (M/ΔM) was above 4500 (e.g. 2 916 was required to resolve mass interference between ^{13}C and $^{12}C^1H$), and mass calibration was achieved using standard iron oxide references. The isotope ratio of the two ^{12}C and ^{13}C carbon isotopes allowed us to localize and quantify the ^{13}C-labeled PHE. The quantitative data acquired by NanoSIMS were calculated with Winimage software that directly processes image data (CAMECA file format) and measures the $\delta^0/_{00}$ isotopic deviation according to the $\delta^0/_{00}$ formula (Eq. 1) for each pixel. The deviation of the $^{13}C/^{12}C$ ratio was calculated based on a fixed R_{ref} value (commonly 1.107%, the natural isotope ratio for ^{13}C). The isotopic ratio of ^{13}C determined by NanoSIMS was not compare to IRMS values because of the presence of the epoxy resin which prevent a specific ^{13}C signal of organic matter (Vidal et al., 2016). The scale of all the images of isotopic map deviation was kept constant (0 to 300) to allow for a quick comparison of intensity levels.

Carbon-to-nitrogen ($^{12}C/^{12}C^{14}N$) and sulfur-to-nitrogen ($^{32}S/^{12}C^{14}N$) ratio data were extracted from regions of interest (ROIs) by using the freeware package Image J. Each ROI was drawn at least twice for each group in order to obtain a mean ratio for any given area. Linescan (=segments of variable length drawn on the ion image) data were also extracted using OpenMIMS plugging with ImageJ software. Preparation and SIMS analyses were carried out

198 with a Cameca NanoSIMS 50 at the Luxembourg Institute of Science and Technology (LIST)
199 in Esch-sur-Alzette, Luxembourg.
200

201 2.4. Statistical analyses

202 Statistical analyses were performed using R software (version 3.1.3, 2015). All tests were
203 used with a 95% significant level. Parametric conditions were checked with Shapiro-Wilk's
204 test for normality and with Bartlett's test for homogeneity of variance. When normality
205 conditions were not met, a non-parametric statistical test was used for multiple comparisons of
206 means. Two-way analysis of variance (ANOVA 2) followed by Tukey's post hoc test was used
207 for the comparison of PHE and ^{13}C concentrations between sampling times and between
208 treatments. For NanoSIMS analysis, the relative abundance levels of ^{13}C from ROI were
209 compared with a non-parametric analysis of variance (Kruskal-Wallis test).
210

211 **3. Results**

212 3.1. Phenanthrene concentrations in planted and non-planted mesocosms

213 The extractable PHE concentration immediately after soil spiking (T0) was 171.6 ± 0.7
214 mg kg^{-1} (Figure 1). After 7 days, PHE concentrations were 128.1 ± 9.7 and 137.6 ± 10.8 mg kg^{-1}
215 in the planted and non-planted mesocosms, respectively, indicating 20-25% PHE dissipation.
216 The main decrease in PHE concentration was noted after 14 days, with 49.8 ± 15.6 and 40.2 ±
217 15.9 mg kg^{-1} of PHE in the planted and non-planted mesocosms, respectively, i.e.
218 approximately 70% of PHE loss. Finally, after 21 days there remained less than 20 mg kg^{-1} of
219 PHE in each mesocosm. The PHE concentration decreased significantly over time: 90% of the

220 added PHE was dissipated after 21 days. No significant difference in PHE concentrations was
221 noted over time between the planted and non-planted mesocosms.

222

223 3.2. ^{13}C-enrichment and distribution in the planted and non-planted mesocosms

224 ^{13}C-enrichment ($E^{13}C$) values are summarized in Table 1 and Figure 2a. No significant
225 difference in $E^{13}C$ was noted between the planted and non-planted mesocosms. $E^{13}C$ of the bulk
226 soil decreased from 0.097 at.% at T0 down to 0.047 at.% after 21 days, while $E^{13}C$ of the
227 residual soil increased from 0.005 at.% to 0.044 at.% over the same time period. At the end of
228 the trial, there was no significant difference in ^{13}C concentration between the bulk and residual
229 soils, indicating that ^{13}C was mainly present in the residual soil under a non-extractable form
230 (Table 1). $E^{13}C$ in plant tissues was studied after 7 days. It reached 0.015 at.% and 0.017 at.%
231 in the roots and shoots, respectively. From 14 days, no significant difference was noted between
232 root and shoot $E^{13}C$ due to the high heterogeneity of values. After 21 days, $E^{13}C$ in residual soil
233 as well as in ryegrass shoots and roots was around 0.04 at.%.

234 ^{13}C distribution was measured over time for the different compartments of the
235 mesocosms: residual soil, PAH extract, plant, and C loss (Figure 2b). At T0, 94% of the total
236 ^{13}C content was recovered in the PAH extract, and 6% in the residual soil. The ^{13}C content of
237 the PAH extract decreased over time down to 3-11% of the total ^{13}C content, while it increased
238 significantly in residual soil and reached 45-48% of the total ^{13}C content after 21 days. The
239 ryegrass ^{13}C content represented less than 1% of the total ^{13}C content, mainly due to the very
240 low dry mass as compared to the total mass of soil (a few mg versus 40 g). The ^{13}C loss from
241 mesocosms accounted for 19% after 7 days and up to 43% after 14 days.

242

243 3.3. Mapping of ^{13}C enrichment in ryegrass roots

244 NanoSIMS analyses were carried out on unlabeled and labeled roots after 7 and 14 days.
245 The mean percentages of ^{13}C atoms in the roots were 1.09 in unlabeled (control) roots, 1.11 in
246 ^{13}C-labeled roots after 7 days, and 1.15 in ^{13}C-labeled roots after 14 days. A significant ^{13}C-
247 enrichment was noted in labeled roots after 14 days relatively to the control.

248 A mapping of ^{13}C associated with ^{12}C, $^{12}C^{14}N$, ^{32}S, $^{56}Fe^{16}O$ ion species was performed on
249 root cross sections after 14 days (Figure 3). The roots were clearly identified in association with
250 high $^{12}C^-$, $^{12}C^{14}N^-$ and $^{32}S^-$ signals. The resin was clearly visible with high $^{12}C^-$ levels but no
251 $^{12}C^{14}N^-$ or $^{32}S^-$ intensity, and was easily differentiated from the root tissue. Mineral particles
252 such as iron oxides, assimilated to soil particles, were highlighted by the $^{56}Fe^{16}O^-$ signal and
253 they were only observed surrounding the root. The composite image resulting from the overlay
254 of ^{12}C, $^{12}C^{14}N$ and ^{13}C elements emphasized ^{13}C enrichment localization. There was no visual
255 evidence of global ^{13}C enrichment in the roots, but rather locally distributed hotspots. Three
256 zones were identified close to the root epidermis (Figure 4), but none close to the soil particles.
257 These hotspots were mainly oval-shaped, and 1 to 2 μm in diameter.

258 An area of interest, pinpointed by the white square in Figure 3, was enlarged and
259 presented in Figure 4.a) Hotspots (red), root (green and blue association), soil (white) and resin
260 (green) were well identified. The black zone between the resin and the root could be holes that
261 formed during sample preparation. The hotspots were adherent to the root epidermal cells but
262 not to the soil particles. A linescan was drawn through root and hotspots (Figure 4.b) to study
263 $^{12}C^-$, $^{13}C^-$, $^{12}C^{14}N^-$ and $^{32}S^-$ distribution. It showed that a higher $^{13}C^-$ signal as compared to $^{12}C^-$ was
264 correlated with a higher $^{32}S^-$ signal as compared to $^{12}C^{14}N^-$. This higher $^{32}S^-$ signal as compared
265 to $^{12}C^{14}N^-$ was not observed in the root but only in the hotspot, so that the hotspots appeared to
266 be made of something else than root tissue. $^{12}C/^{12}C^{14}N$, $^{32}S/^{12}C^{14}N$ and $^{56}Fe^{16}O/^{12}C$ ratios were
267 also calculated for ROI selection in the hotspots, root tissue, soil particles and resin (Table 2).

Hotspots were easily discriminated from roots because they displayed significantly higher $^{12}C/^{12}C^{14}N$ and $^{32}S/^{12}C^{14}N$ ratios. They were not considered as soil particles because they had a low $^{56}Fe^{16}O/^{12}C$ ratio, or as resin because they contained less C than resin ($^{12}C/^{12}C^{14}N$ ratios equivalent to 12.88 for resin and 1.02 for hotspots).

4. Discussion

4.1. Effect of the rhizosphere on phenanthrene degradation

The extractable PHE concentration decreased by 40% after spiking and by up to 90% after 21 days in the planted and non-planted systems (Figure 1). This rapid dissipation of PHE and its high rate are in part explained by experimental conditions, including the high bioavailability of the freshly spiked pollutant and soil inoculation with adapted microflora. Smith et al. (2011) showed that using a soil freshly spiked with pure PAH led to a greater loss than using historically contaminated soils. Inoculation of a microflora extracted from PAH-contaminated soil had a priming effect in the first days following contamination and increased PHE degradation (Joner et al., 2004, 2002). Low-molecular-weight PAHs such as PHE (3 rings) can be used as primary substrates and be easily broken down in the soil by adapted microflora commonly found in polluted soils (Cerniglia, 1997). This rapid PHE degradation could mask a potential rhizospheric effect, even in a forest soil. No significant difference was noted in ^{13}C-dynamics between the planted and non-planted systems (Figure 2). Therefore there is no evidence of an impact of the rhizosphere on PAH degradation in this type of plant-soil mesocosm.

4.2. Dynamics of phenanthrene carbon in the plant-soil mesocosms

The dynamics of PHE degradation was studied by monitoring the increase in C loss and C incorporation in the soil (Figure 2.a). The loss of ^{13}C during the first 14 days

represented half of the spiked ^{13}C (Figure 2.b). We hypothesized that a major part of the PHE loss was mineralized as CO_2. There was no significant difference in PHE degradation between 14 and 21 days, which means that PHE degradation occurred during the first days of contamination.

After 14 days, almost 40% of PHE carbon had been incorporated in the soil. This result is in accordance with the 38% of 13C remaining in the soil after 12 days in comparable soil mesocosms used to identify PAH-degrading bacteria (Cébron et al., 2011). No PHE metabolite, like those identified by Käcker et al. (2002) and Richnow et al. (2000) for example, was detected by GC-MS analysis of PAH extracts. The remaining 13C incorporated in the soil must then have been present under the form of other organic compounds that were not extracted by dichloromethane. Kästner et al. (1999) conducted a long-term experiment on the transformation of 13C-labeled PAHs in soil bioreactors; they highlighted that the non-extractable residue had a relatively high stability over time. These organic compounds, newly formed from PAHs, become soil-bound residues (Binet et al., 2000) and/or a C source for microorganisms (Richnow et al., 1998; 2000). For Richnow et al. (1999), the formation of these compounds most probably depends on an intense microbial activity. Soil microorganisms may use organic pollutants like PAHs as a C source and transform them into biomass through anabolic processes. Part of these newly formed compounds can also be incorporated into organo-mineral complexes and be protected against degradation depending on the nature of mineral phases (de Junet et al., 2013). This could explain why these organic compounds remain non-available in the soil (Macleod and Semple, 2003; Pignatello and Xing, 1996) and have a relative high stability (Richnow et al., 1999).

Less than 1% of total PHE carbon was taken up by ryegrass roots and shoots. No significant difference was noted between the two plant parts after 14 and 21 days. Plant ^{13}C enrichment was similar to soil ^{13}C enrichment, namely about 0.04 at.% (Figure 2a), and

317 the difference expressed in total amounts was only due to the difference in mass between
318 the soil and the plants. However, according to NanoSIMS analyses (Figure 4), there was
319 no evidence of direct PHE uptake by plant roots. A small part of PHE may have been
320 sorbed onto the root epidermis, more precisely near the suberized exodermis and
321 endodermis (Dupuy et al., 2016). Previous studies show preferential PAH incorporation in
322 shoots through atmospheric deposition, and low direct incorporation by roots (Binet et al.,
323 2000a; Desalme et al., 2011; Schwab and Banks, 1994). If ^{13}C was not taken up by the
324 roots under the form of PHE, it may have been taken up under the form of newly formed
325 organic compounds or ^{13}C-CO_2. It could be absorbed or adsorbed from ambient air by the
326 shoots after PHE volatilization (Gao and Zhu, 2004) or through stomata under the form of
327 ^{13}C-CO_2 during the photosynthetic process. 13C enrichment was also noted in roots by SIMS,
328 confirming the excess ^{13}C recovered in the roots (Figure 2.a).
329

330 4.3. Determination of ^{13}C hotspots and localization of ^{13}C in ryegrass roots

331 There was no correlation between the $^{56}Fe^{16}O$ and ^{13}C signals close to the roots after 14
332 days, therefore SIMS analyses did not evidence any contribution of organic matter-mineral
333 associations to the ^{13}C-PAH dynamics. However two types of enrichment were highlighted
334 in the plant rhizosphere: a global ^{13}C enrichment and ^{13}C hotspots. Hotspots were composed
335 of $^{12}C^-$, $^{12}C^{14}N^-$ and $^{32}S^-$ ions species. Sulfur and nitrogen contents suggest the presence of
336 proteins (Eybe et al., 2008) that could originate from the plants or from microorganisms.
337 Hotspots were discriminated from root tissues based on their high ^{32}S content as compared to
338 the roots (Figure 4 and Table 2). The $^{32}S/^{12}C^{14}N$ ratio of the hotspots (0.11) was around five
339 times higher than the $^{32}S/^{12}C^{14}N$ ratio of the ryegrass roots (0.02). This last value is in
340 accordance with the $^{32}S/^{12}C^{14}N$ ratio of 0.027 found by Dijkshoorn and Van Wijk (1967) in
341 ryegrass shoots. The oval shape of the hotspots and their size (1 to 2 μm in diameter) are in

accordance with the shape and size of bacteria. Moreover, measurements were performed on isolated bacteria (unpublished data) and showed similar ratios (0.1 for $^{32}S/^{12}C^{14}N$). There was evidence of global ^{13}C enrichment during plant growth, but no PAH uptake by the roots was visualized by NanoSIMS analyses (Figure 4). The main ^{13}C-PAH uptake could be attributed to the bacteria present in the rhizospheric environment.

5. Conclusion

A mesocosm experiment was conducted using ^{13}C-phenanthrene to monitor the dynamics of PHE and derived compounds in the soil and in ryegrass. After 21 days, almost 90% of spiked PHE had been degraded. PHE was mainly mineralized under gas phase (up to 53%, corresponding to the ^{13}C loss). But after 14 days, more than 40% of PHE carbon had been transformed into newly formed organic compounds (metabolites) or incorporated into the microbial biomass. No rhizospheric effect on PAH dynamics was noted due to the rapid dissipation of PHE. Less than 1% of PHE carbon was also found in the root and shoot tissues of ryegrass. The plant $E^{13}C$ was similar to the soil $E^{13}C$ (~ 0.04 at.%), suggesting a homogeneous C-PAH distribution in the plant-soil mesocosm.

Global root C-PAH enrichment was also determined in the ryegrass rhizosphere at a finer scale using NanoSIMS, based on $^{13}C/^{12}C$ ratio measurements on images obtained for control (^{12}C) and labeled samples after 7 and 14 days. There was no evidence of ^{13}C-PAH association to iron oxides in the close root environment. However, hotspots of ^{13}C enrichment close to the roots probably indicated the presence of bacteria, as suggested by their size, shape and element composition. A part of PAH carbon was sorbed on the roots, but it was mainly incorporated into the bacteria mentioned above. These bacteria probably degraded PHE and incorporated PHE-derived ^{13}C into their biomass.

366 The use of labeled contaminants and the coupling of IRMS and NanoSIMS is a relevant
367 and powerful tool for determining the dynamics of these contaminants. The dynamics of ^{13}C
368 from labeled PAH was highlighted by ^{13}C-partionning at a global level, but the transformation
369 of PAH ^{13}C at a molecular level remains to be investigated. Complementary techniques such as
370 ^{13}C-NMR and pyGCMS could be used to further characterize the ^{13}C-PAH metabolites.
371
372 **Acknowledgements**
373 This work was supported by a grant from the University of Lorraine and the Lorraine
374 Region. The authors thank David Billet for UHPLC analyses and Patrick Grysan for NanoSIMS
375 analyses.
376

377 ## References

378 Anderson, T.A., Guthrie, E., Walton, B.T., 1993. Bioremediation in the rhizosphere. Environ.
379 Sci. Technol. 27, 2630–2636. doi:10.1021/es00049a001
380 Behrens, S., Lösekann, T., Pett-Ridge, J., Weber, P.K., Ng, W.O., Stevenson, B.S., Hutcheon,
381 I.D., Relman, D.A., Spormann, A.M., 2008. Linking microbial phylogeny to metabolic
382 activity at the single-cell level by using enhanced element labeling-catalyzed reporter
383 deposition fluorescence in situ hybridization (EL-FISH) and NanoSIMS. Appl. Environ.
384 Microbiol. 74, 3143–3150. doi:10.1128/AEM.00191-08
385 Binet, P., Portal, J.M., Leyval, C., 2000a. Fate of polycyclic aromatic hydrocarbons (PAH) in
386 the rhizosphere and mycorrhizosphere of ryegrass. Plant Soil 227, 207–213.
387 doi:10.1023/A:1026587418611
388 Binet, P., Portal, J.M., Leyval, C., 2000b. Dissipation of 3–6-ring polycyclic aromatic
389 hydrocarbons in the rhizosphere of ryegrass. Soil Biol. Biochem. 32, 2011–2017.
390 doi:10.1016/S0038-0717(00)00100-0

391 Burken, J.G., Schnoor, J.L., 1998. Predictive relationships for uptake of organic contaminants
392 by hybrid poplar trees. Environ. Sci. Technol. 32, 3379–3385. doi:10.1021/es9706817
393 Cébron, A., Louvel, B., Faure, P., France-Lanord, C., Chen, Y., Murrell, J.C., Leyval, C., 2011.
394 Root exudates modify bacterial diversity of phenanthrene degraders in PAH-polluted soil
395 but not phenanthrene degradation rates. Environ. Microbiol. 13, 722–736.
396 doi:10.1111/j.1462-2920.2010.02376.x
397 Cerniglia, C.E., 1997. Fungal metabolism of polycyclic aromatic hydrocarbons: past, present
398 and future applications in bioremediation. J. Ind. Microbiol. Biotechnol. 19, 324–33.
399 Corgié, S.C., Joner, E.J., Leyval, C., 2003. Rhizospheric degradation of phenanthrene is a
400 function of proximity to roots. Plant Soil 257, 143–150. doi:10.1023/A:1026278424871
401 de Junet, A., Basile-Doelsch, I., Borschneck, D., Masion, A., Legros, S., Marol, C., Balesdent,
402 J., Templier, J., Derenne, S., 2013. Characterisation of organic matter from organo-mineral
403 complexes in an Andosol from Reunion Island. J. Anal. Appl. Pyrolysis 99, 92–100.
404 doi:10.1016/j.jaap.2012.10.020
405 Desalme, D., Binet, P., Bernard, N., Gilbert, D., Toussaint, M.L., Chiapusio, G., 2011.
406 Atmospheric phenanthrene transfer and effects on two grassland species and their root
407 symbionts: a microcosm study. Environ. Exp. Bot. 71, 146–151.
408 doi:10.1016/j.envexpbot.2010.11.009
409 Dijkshoorn.W., Van Wijk.L., 1967. The sulphur requirements of plants evidenced by the
410 sulphur-nitrogen ratio in the organic matter a review of published data. Plant Soil 26, 129–
411 157.
412 Doick, K.J., Burauel, P., Jones, K.C., Semple, K.T., 2005. Distribution of aged 14C-PCB and
413 14C-PAH residues in particle-size and humic fractions of an agricultural soil. Environ.
414 Sci. Technol. 39, 6575–6583. doi:10.1021/es050523c
415 Dupuy, J., Leglize, P., Vincent, Q., Zelko, I., Mustin, C., Ouvrard, S., Sterckeman, T., 2016.

Effect and localization of phenanthrene in maize roots. Chemosphere 149, 130–136. doi:10.1016/j.chemosphere.2016.01.102

Edwards, N.T., 1983. Polycyclic Aromatic Hydrocarbons (PAH's) in the Terrestrial Environment - A Review. J. Environ. Qual. 12, 427–441. doi:10.2134/jeq1983.00472425001200040001x

Eschenbach, A., Wienberg, R., Mahro, B., 1998. Fate and stability of nonextractable residues of [14 C] in contaminated soils under environmental stress conditions. Environ. Sci. Technol. 32, 2585–2590. doi:10.1021/es9708272

Eybe, T., Audinot, J.N., Bohn, T., Guignard, C., Migeon, H.N., Hoffmann, L., 2008. NanoSIMS 50 elucidation of the natural element composition in structures of cyanobacteria and their exposure to halogen compounds. J. Appl. Microbiol. 105, 1502–1510. doi:10.1111/j.1365-2672.2008.03870.x

Fang, C., Radosevich, M., Fuhrmann, J.J., 2001. Atrazine and phenanthrene degradation in grass rhizosphere soil. Soil Biol. Biochem. 33, 671–678. doi:10.1016/S0038-0717(00)00216-9

Gao, Y., Zhu, L., 2004. Plant uptake, accumulation and translocation of phenanthrene and pyrene in soils. Chemosphere 55, 1169–78. doi:10.1016/j.chemosphere.2004.01.037

Günther, T., Dornberger, U., Fritsche, W., 1996. Effects of ryegrass on biodegradation of hydrocarbons in soil. Chemosphere 33, 203–215. doi:10.1016/0045-6535(96)00164-6

Hartmann, R., 1996. Polycyclic aromatic hydrocarbons (PAHs) in forest soils: Critical evaluation of a new analytical procedure. Int. J. Environ. Anal. Chem. 62, 161–173. doi:10.1080/03067319608027062

Herrmann, A.M., Ritz, K., Nunan, N., Clode, P.L., Pett-Ridge, J., Kilburn, M.R., Murphy, D. V., O'Donnell, A.G., Stockdale, E.A., 2007. Nano-scale secondary ion mass spectrometry - A new analytical tool in biogeochemistry and soil ecology: A review article. Soil Biol.

441 Biochem. 39, 1835–1850. doi:10.1016/j.soilbio.2007.03.011
442 Hoppe, P., Cohen, S., Meibom, A., 2013. NanoSIMS: technical aspects and applications in
443 cosmochemistry and biological geochemistry. Geostand. Geoanalytical Res. 37, 111–154.
444 doi:10.1111/j.1751-908X.2013.00239.x
445 Hwang, S., Cutright, T.J., 2002. Biodegradability of aged pyrene and phenanthrene in a natural
446 soil. Chemosphere 47, 891–899. doi:10.1016/S0045-6535(02)00016-4
447 Joner, E.J., Corgie, S.C., Amellal, N., Leyval, C., 2002. Nutritional constraints to degradation
448 of polycyclic aromatic hydrocarbons in a simulated rhizosphere. Soil Biol. Biochem. 34,
449 859–864. doi:10.1016/S0038-0717(02)00018-4
450 Joner, E.J., Hirmann, D., Szolar, O.H.J., Todorovic, D., Leyval, C., Loibner, A.P., 2004.
451 Priming effects on PAH degradation and ecotoxicity during a phytoremediation
452 experiment. Environ. Pollut. 128, 429–35. doi:10.1016/j.envpol.2003.09.005
453 Käcker, T., Haupt, E.T.K., Garms, C., Francke, W., Steinhart, H., 2002. Structural
454 characterisation of humic acid-bound PAH residues in soil by 13C-CPMAS-NMR-
455 spectroscopy: Evidence of covalent bonds. Chemosphere 48, 117–131.
456 doi:10.1016/S0045-6535(02)00082-6
457 Kästner, M., Streibich, S., Beyrer, M., Richnow, H.H., Ka, M., 1999. Formation of bound
458 residues during microbial degradation of [14 C] anthracene in soil. Appl. Environ.
459 Microbiol. 65, 1834–1842. doi:0099-2240/99/$04.00+0
460 Kipopoulou, A.M., Manoli, E., Samara, C., 1999. Bioconcentration of polycyclic aromatic
461 hydrocarbons in vegetables grown in an industrial area. Environ. Pollut. 106, 369–80.
462 Liste, H.H., Alexander, M., 2000. Plant-promoted pyrene degradation in soil. Chemosphere 40,
463 7–10. doi:10.1016/S0045-6535(99)00216-7
464 Macleod, C.J.A., Semple, K.T., 2003. Sequential extraction of low concentrations of pyrene
465 and formation of non-extractable residues in sterile and non-sterile soils. Soil Biol.

466 Biochem. 35, 1443–1450. doi:10.1016/S0038-0717(03)00238-4
467 Magee, B.R., Lion, L.W., Lemley, A.T., 1991. Transport of dissolved organic macromolecules
468 and their effect on the transport of phenanthrene in porous media. Environ. Sci. Technol.
469 25, 323–331. doi:10.1021/es00014a017
470 Miya, R.K., Firestone, M.K., 2000. Phenanthrene-degrader community dynamics in
471 rhizosphere soil from a common annual grass. J. Environ. Qual. 29, 584.
472 doi:10.2134/jeq2000.00472425002900020029x
473 Moore, K.L., Lombi, E., Zhao, F.J., Grovenor, C.R.M., 2012. Elemental imaging at the
474 nanoscale: NanoSIMS and complementary techniques for element localisation in plants.
475 Anal. Bioanal. Chem. 402, 3263–3273. doi:10.1007/s00216-011-5484-3
476 Northcott, G.L., Jones, K.C., 2001. Partitioning, extractability, and formation of non extractable
477 PAH residues in soil.2. Effects on compund dissolution bahaviour. Environ. Sci. Technol.
478 35, 1111–1117. doi:10.1021/es000072q
479 Pignatello, J.J., Xing, B., 1996. Mechanisms of slow sorption of organic chemicals to natural
480 particles. Environ. Sci. Technol. 30, 1–11. doi:10.1021/es940683g
481 Printz, B., Guerriero, G., Sergeant, K., Audinot, J.-N., Guignard, C., Renaut, J., Lutts, S.,
482 Hausman, J.-F., 2016. Combining-omics to unravel the impact of copper nutrition on
483 Alfalfa (Medicago sativa) stem metabolism. Plant Cell Physiol. 57, 407–22.
484 doi:10.1093/pcp/pcw001
485 Reilley, K.A., Banks, M.K., Schwab, A.P., 1996. Dissipation of polycyclic aromatic
486 hydrocarbons in the rhizosphere. J. Environ. Qual. 25, 212.
487 doi:10.2134/jeq1996.00472425002500020002x
488 Remusat, L., Hatton, P., Nico, P.S., Zeller, B., Kleber, M., Derrien, D., 2012. NanoSIMS study
489 of organic matter associated with soil aggregates: advantages, limitations, and
490 combination with STXM. Environ. Sci. Technol. 46, 3943–3949. doi:10.1021/es203745k

491 Rezek, J., in der Wiesche, C., Mackova, M., Zadrazil, F., Macek, T., 2008. The effect of
492 ryegrass (Lolium perenne) on decrease of PAH content in long term contaminated soil.
493 Chemosphere 70, 1603–8. doi:10.1016/j.chemosphere.2007.08.003
494 Richnow, H.H., Annweiler, E., Koning, M., Lüth, J.C., Stegmann, R., Garms, C., Francke, W.,
495 Michaelis, W., 2000a. Tracing the transformation of labelled [1-13C]phenanthrene in a
496 soil bioreactor. Environ. Pollut. 108, 91–101. doi:10.1016/S0269-7491(99)00205-5
497 Richnow, H.H., Eschenbach, A., Mahro, B., Kästner, M., Annweiler, E., Seifert, R., Michaelis,
498 W., 1999. Formation of nonextractable soil residues: A stable isotope approach. Environ.
499 Sci. Technol. 33, 3761–3767. doi:10.1021/es980927n
500 Richnow, H.H., Eschenbach, A., Mahro, B., Seifert, R., Wehrung, P., Albrecht, P., Michaelis,
501 W., 1998. The use of 13C-labelled polycyclic aromatic hydrocarbons for the analysis of
502 their transformation in soil. Chemosphere 36, 2211–2224. doi:10.1016/S0045-
503 6535(97)10193-X
504 Sabaté, J., Viñas, M., Solanas, A.M., 2006. Bioavailability assessment and environmental fate
505 of polycyclic aromatic hydrocarbons in biostimulated creosote-contaminated soil.
506 Chemosphere 63, 1648–1659. doi:10.1016/j.chemosphere.2005.10.020
507 Schwab, A.P., Banks, M.K., 1994. Biologically mediated dissipation of polyaromatic
508 hydrocarbons in the root zone. Am. Chem. Soc. doi:10.1021/bk-1994-0563.ch012
509 Smith, M.J., Flowers, T.H., Duncan, H.J., Saito, H., 2011. Study of PAH dissipation and
510 phytoremediation in soils: comparing freshly spiked with weathered soil from a former
511 coking works. J. Hazard. Mater. 192, 1219–1225. doi:10.1016/j.jhazmat.2011.06.033
512 Vidal, A., Remusat, L., Watteau, F., Derenne, S., Quenea, K., 2016. Incorporation of 13C
513 labelled shoot residues in Lumbricus terrestris casts: A combination of transmission
514 electron microscopy and nanoscale secondary ion mass spectrometry. Soil Biol. Biochem.
515 93, 8–16. doi:10.1016/j.soilbio.2015.10.018

516 Wilson, S.C., Jones, K.C., 1993. Bioremediation of soil contaminated with polynuclear
517 aromatic hydrocarbons (PAHs): a review. Environ. Pollut. 81, 229–249.
518 doi:10.1016/0269-7491(93)90206-4
519
520

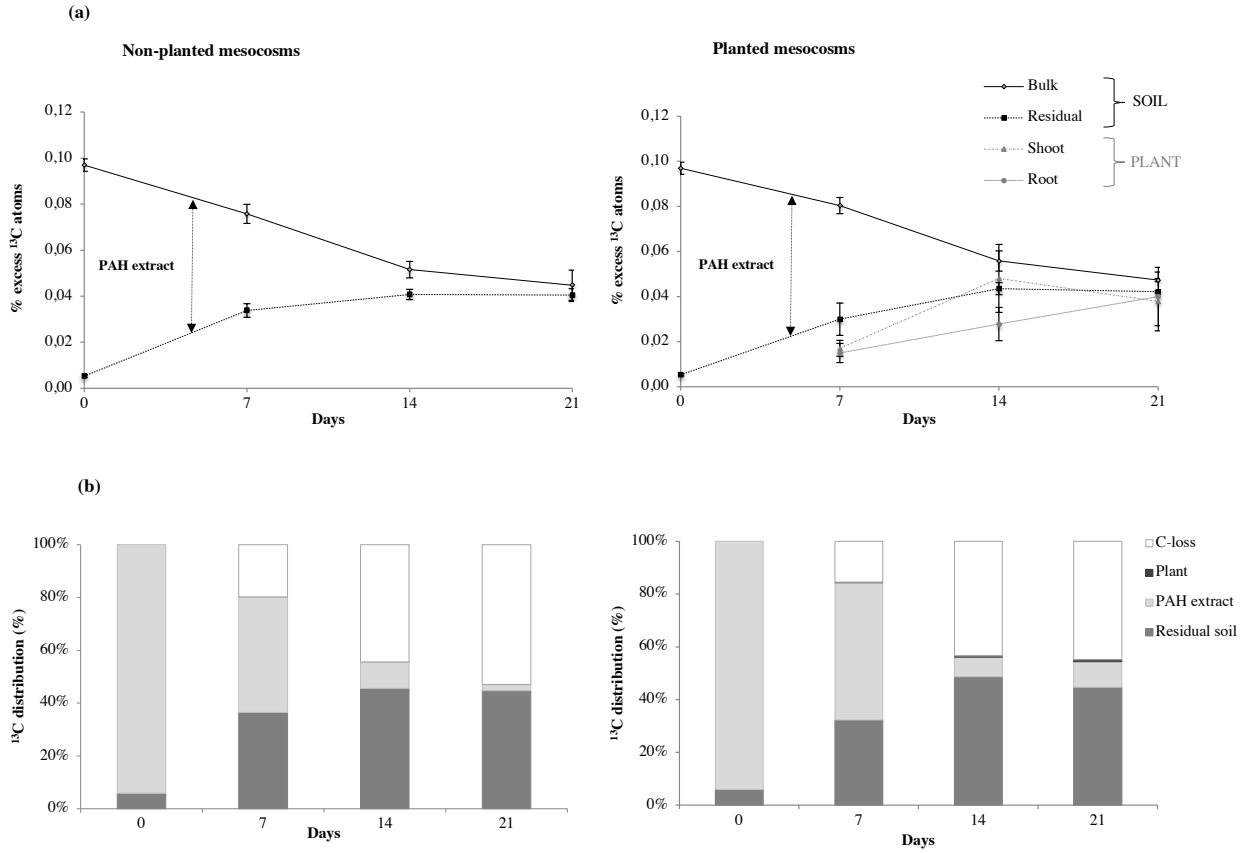

521

522 **Figure 1**. Extractable concentrations of phenanthrene (PHE, mg kg^{-1} of soil) in planted and
523 non-planted mesocosms at different time-points over a 21-day period. Means ± SD, n = 4.
524 Different letters indicate significant differences ($p<0.05$) between the sampling times.

525

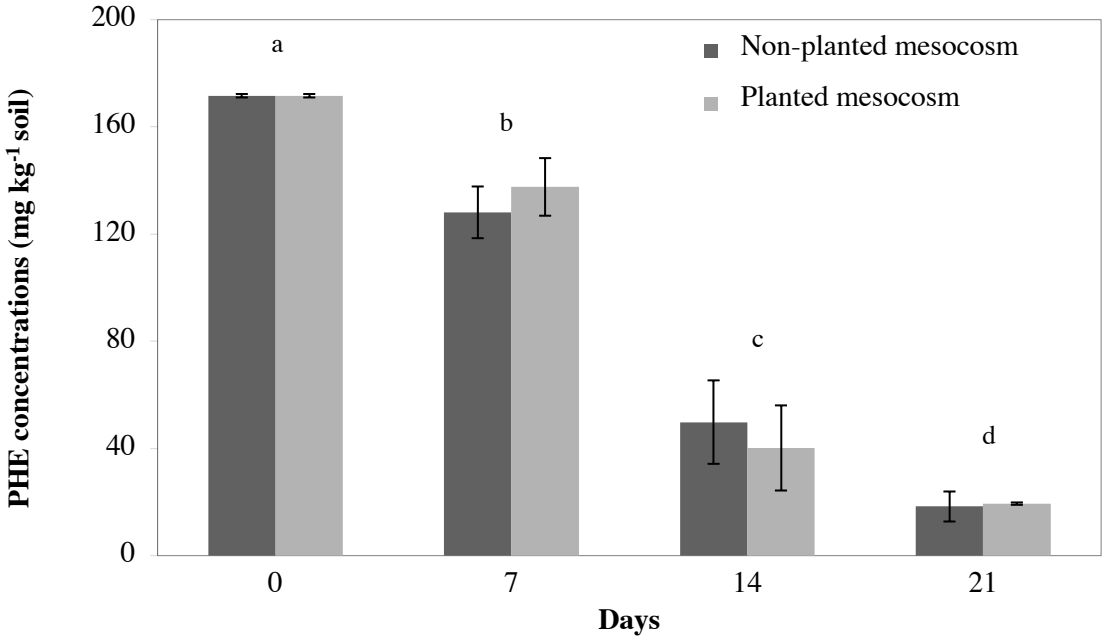

526

527 **Figure 2.** ^{13}C dynamics after ^{13}C-PHE spiking in non-planted (left) and planted (right)
528 mesocosms at different time-points over a 21-day period. **(a)** ^{13}C enrichment ($E^{13}C$, at.%) in the
529 plant and soil compartments. Means ± SD, n = 4. ^{13}C enrichment was calculated from $\delta^{13}C$ data
530 obtained by EA-IRMS. (**b)** ^{13}C distribution in the mesocosm compartments (PAH extract,
531 residual soil, plant, and C loss). Results are expressed as percentages of the ^{13}C-PHE
532 concentrations initially added in the soil. The plant compartment gathers root and shoot data.
533 PAH extract concentrations were calculated as the difference between bulk and residual soil
534 concentrations**.**

535

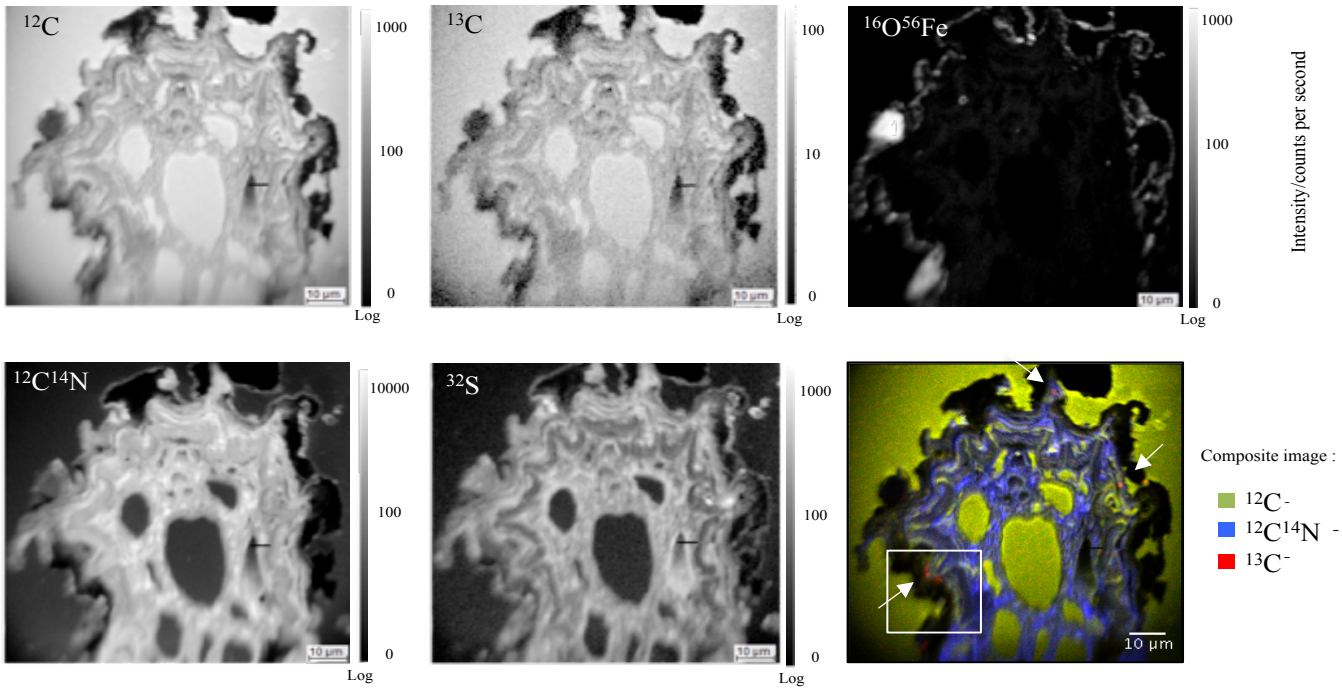

Figure 3. NanoSIMS elemental maps of $^{12}C^-$, $^{13}C^-$, $^{12}C^{14}N^-$, $^{32}S^-$ and $^{56}Fe^{16}O^-$ from labeled ryegrass roots after 14 days. The 90*90-μm^2 images are cross views of whole roots with adherent soil particles. A composite image (bottom right) was obtained by overlaying the $^{12}C^-$, $^{12}C^{14}N^-$ and $^{13}C^-$ images. Three areas of interest (bordered in white) with higher ^{13}C content were identified. NanoSIMS data were analyzed using Winimage software.

555

556

(a) (b)

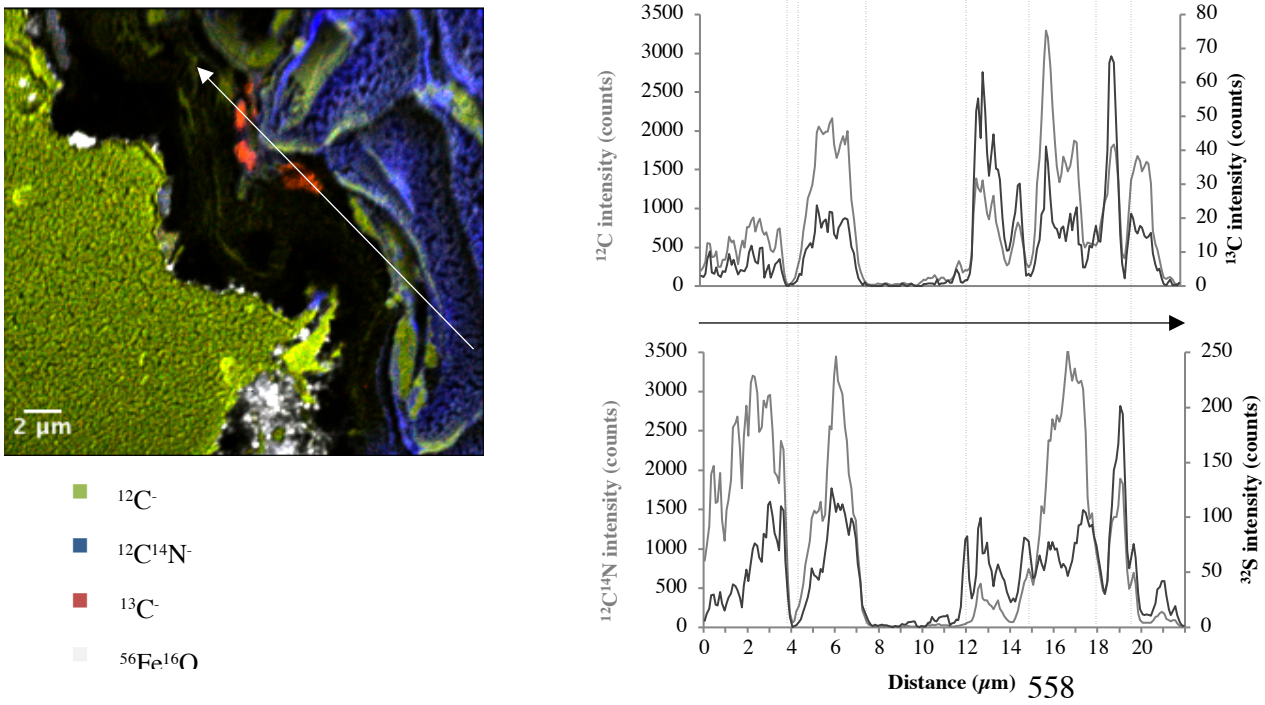

557 558

559

560

561 **Figure 4.** NanoSIMS composite image and linescan obtained from root tissue after 14 days.

562 The zone is located inside the white square of Figure 3. (a) Composite 25*25-μm^2 image with

563 hotspots reflecting the ^{13}C-enrichment (red) obtained by overlaying $^{12}C^-$, $^{13}C^-$, $^{12}C^{14}N^-$ and

564 $^{56}Fe^{16}O^-$ (white) ion species images. (b) A white segment was drawn through these hotspots

565